Formation of delta ferrite in 9 wt.% Cr steel investigated by in-situ X-ray diffraction using synchrotron radiation

P. Mayr[1,2], T.A. Palmer[3], J.W. Elmer[4], E.D. Specht[5], S.M. Allen[1]

[1] Department of Materials Science and Engineering, Massachusetts Institute of Technology, 77 Massachusetts Av., Cambridge, MA 02139, USA

[2] Institute for Materials Science and Welding, Graz University of Technology, Kopernikusgasse 24, 8010 Graz, Austria

[3] Department of Materials Science and Engineering, Penn State University, University Park, PA 16802, USA

[4] Lawrence Livermore National Laboratory, Livermore, CA, USA

[5] Oak Ridge National Laboratory, Oak Ridge, TN 37831, USA

Keywords: martensitic steel, X-ray diffraction, phase transformations, delta ferrite

Abstract

In-situ X-ray diffraction measurements using high energy synchrotron radiation were performed to monitor in real time the formation of delta ferrite in a martensitic 9wt.% chromium steel under simulated weld thermal cycles. Volume fractions of martensite, austenite and delta ferrite were measured as a function of temperature at a 10K/s heating rate to 1573K (1300°C) and subsequent cooling. At the peak temperature, the delta ferrite concentration rose to 19%, of which 17% transformed back to austenite on subsequent cooling.

Introduction

Cast martensitic 9 - 12 wt. % chromium steels are widely used for thick-walled high-temperature turbine casings or steam valves in thermal power generation. The chemical composition is carefully balanced between austenite (γ) stabilizing elements (C, Mn, Ni, Co, Cu, and N) and ferrite (α) stabilizers (Si, Cr, W, Mo, V, and Nb) to avoid the presence of stable delta ferrite (δ) at room temperature and the accompanying reduced toughness and ductility [1].

After welding, δ-ferrite is often retained in the heat-affected zone of the base material adjacent to the weld fusion line [3]. This region is exposed to peak temperatures just below the melting temperature for prolonged periods,

promoting the formation of high-temperature phases. Little is known about the formation of δ-ferrite, its phase fraction evolution during weld thermal cycles and the mechanism of retention in a former δ-ferrite free martensitic steel. In this investigation, the formation and dissolution of δ-ferrite in a 9 wt. % chromium steel is monitored using in-situ X-ray diffraction with synchrotron radiation during exposure to a single-weld thermal cycle. These results are then analyzed using thermodynamic equilibrium calculations, dilatometry, metallography and optical phase fraction analysis.

Material

A 100 kg ingot of an experimental Fe-0.168C-0.23Si-0.22Mn-8.85Cr-1.54Mo-0.18Ni-0.29V-0.057Nb-0.009B-0.016N steel (wt.%) was produced by conventional sand casting. It was normalized at 1373K (1100°C) for 8 hours and after air-cooling to room temperature tempered at 1003K (730°C) for 10 hours, allowed to air cool to room temperature, and tempered again for an additional 24 hours at this same temperature. A tempered martensite microstructure with no delta ferrite was observed. Finely dispersed precipitates were identified by analytical transmission electron microscopy as Cr-rich $M_{23}C_6$ carbides, V-rich MX nitrides and Nb-rich MX carbides.

Results and Discussion

An equilibrium phase diagram (Figure 1) was calculated using Matcalc® [4] with the MC_steel database [5]. At the nominal Cr content (8.85 wt.%), equilibrium phase transformation temperatures are predicted at A_{e1}=1113K (840°C), A_{e3}=1168K (895°C), A_{e4}=1497K (1224°C), where A_{e1} indicates the onset of austenite formation, A_{e3} the achievement of a fully austenitic state and A_{e4} the start of δ-ferrite formation on heating. During cooling, the steel passes through the single-phase austenite (γ) region and a fully martensitic microstructure with no stable δ-ferrite at room temperature is formed after it passes through the martensite start temperature (M_S) at 697K (424°C) and cools to room temperature.[6] As indicated by a dashed vertical line in Figure 1, increasing the chromium content beyond 11.4 wt. % would result in bypassing the single-phase γ region and permit a certain amount of stable δ-ferrite embedded in a martensitic matrix to be present at room temperature.

Figure 1: Calculated isopleth for a martensitic steel with the chemical composition given above but allowing the chromium content to range from 6 to 16 wt. %.

In-situ X-ray diffraction experiments were performed at beamline 33-BM-C of the Advanced Photon Source at Argonne National Laboratory using a 30 keV X-ray beam. Test coupons measuring 100 mm long by 4.75 mm wide by 2 mm thick were heated at a rate of 10 Ks^{-1} to a peak temperature (T_P) of 1573K (1300°C), where it is held for 3 seconds and then cooled at the same rate to room temperature in an evacuated specimen chamber. Direct resistance heating was used to achieve the desired thermal cycle in the specimen. This temperature profile is similar to a

thermal cycle experienced in the heat-affected zone adjacent to the weld fusion line. A schematic of the experimental setup is given in Figure 2. The heating rate was reduced in order to acquire sufficient diffraction patterns to be recorded during heating. Further details regarding the experimental setup are described elsewhere [7].

Figure 2: Schematic of the experimental setup for the in-situ X-ray diffraction experiments using synchrotron radiation during direct resistance heating of the specimen.

The sample was scanned at 3-second intervals between d-spacing values of 1.1 to 2.3 Å, allowing three Debye arcs representing the austenite phase and three arcs representing the ferrite/martensite phase to be monitored. The Debye arcs were then converted into a 1-D plot showing intensity versus d-spacing. The amounts of austenite and ferrite/martensite present at each time increment are then calculated using an analysis of the peaks present in each diffraction pattern and plotted as a function of time. A detailed description of the method is given elsewhere [8]. With this experimental setup the X-rays don't penetrate very deeply so that mainly surface layers of martensite, austenite and δ-ferrite are studied. For validation of the x-ray diffraction results and generation of additional specimens for further metallographic investigations, dilatometric experiments were performed using a Bähr DIL-805 A/D horizontal dilatometer and solid cylindrical specimens (4 x 10 mm).

Figures 3(a) through 3(c) summarize the sequence of observed phase transformations during the applied thermal cycle in a d-spacing vs. time plot for the ferrite/martensite BCC-BCT (110) and the austenite FCC (111) diffraction peaks and the calculated ferrite/martensite phase fractions. The difference in the lattice constants for the BCC and BCT phases is very small, making it impossible to differentiate between ferrite and martensite using only the XRD results. It was therefore assumed that during cooling all of the BCC diffraction peaks represent the δ-ferrite until the M_s temperature was reached. At this point, the amount of δ-ferrite had decreased to 2 %, and the increase of BCC/BCT peaks as the temperature decreased below M_S was attributed solely to the formation of martensite.

Temperatures at which phase transformations occur were defined as where either 1% of a phase has formed (A_{C1}, $A_{C4,}$ M_S) or 99% of the transformation has been completed (A_{C3}). Table 1 provides a summary of the calculated equilibrium temperatures for these selected transformation temperatures and compares them with the experimental results from the XRD and dilatometry experiments.

Table 1: Comparison of calculated equilibrium and measured phase transformation temperatures during thermal cycling to a peak temperature of 1573K (1300°C) at $10Ks^{-1}$.

In-situ XRD shows, phase transformation of the tempered martensitic to a uniform austenitic structure occurs at temperatures between 1153±15K (880±15°C) (A_{C1}) and 1305±15K (1032 ±15°C) (A_{C3}). The uncertainty in measured transformation temperatures arises from the linear interpolation between two measured values at a 3 second interval (ΔT=30K). In the temperature range from 1305±15K (1032 ±15°C) to 1483±15K (1210±15°C), the steel exhibits a single-phase austenite lattice structure. At 1483±15K (1210±15°C) (A_{C4}), the formation of δ-ferrite is initiated and a phase fraction of 19 % is reached at a temperature of 1573K (1300°C). On cooling, δ-ferrite transforms back to austenite but this transformation is incomplete and results in the retention of about 2% of δ-ferrite

before the martensitic transformation starts. The first formation of martensite is observed at 676±5K (403±5°C) (M_S). The level of uncertainty is reduced to ±5K due to a decrease in cooling rate (3s~ΔT=10K) in this region. When room temperature is reached, about 4% of austenite has not transformed to martensite and is retained.

Dilatometric measurements using a heating rate of $10Ks^{-1}$ confirm the XRD results. In these measurements, the start of δ-ferrite formation occurs at 1260°C. Due to the lower sensitivity of dilatometric measurements, this temperature has a higher, but not quantifiable, degree of uncertainty. The presence of retained δ-ferrite and austenite can also not be determined. Dilatometry showed A_{C1} temperature to be 1165K (892°C), A_{C3} 1303K (1030°C), A_{C4} 1533K (1260°C) and M_S at 713K (440°C). Measured values differ from the calculated equilibrium values due to the strong kinetic influence of heating and cooling rates on the phase transformations.

Optical micrographs (Figure 4) of the sample after thermal cycling revealed a martensitic microstructure with retained δ-ferrite in two morphologies. The first is a skeletal morphology approximately 50 to 100 μm wide and several hundred μm long. This skeletal δ-ferrite has its origin in the formation of small stable homogeneous δ-ferrite grains at or near the peak temperature. When reaching the A_{c4} temperature, δ-ferrite nucleates at the austenite grain boundaries and with further heating experiences a diffusion-governed growth, resulting in single equiaxed δ-ferrite grains in the austenitic matrix.

On cooling, δ-ferrite incompletely re-transforms to austenite leaving a skeletal shaped network of retained δ-ferrite. In this investigation, 17% of the δ-ferrite present at its maximum re-transformed to austenite on cooling, while 2% is retained. The skeletal morphology can be explained by preferred directions of the diffusion-governed δ-ferrite to austenite transformation. Figure 4b shows, based on the etching response of the microstructure, the assumed δ-ferrite grain boundary at high temperature and arrows indicate the progression of the diffusion governed δ-ferrite to austenite transformation leaving a skeletal shaped retained δ-ferrite.

The second morphology of δ-ferrite has a shell-like shape, only a few μm in width, surrounding prior austenite grains. These prior austenite grains with an average diameter of about 100 μm are the result of the initial ferrite to austenite transformation on heating. δ-ferrite formation starts at the prior austenite grain boundaries and proceeds faster in the direction of the grain boundary compared to the grain interior due to enhanced diffusivity along the grain boundary. On cooling, not all of the δ-ferrite transforms back to austenite and a shell-like structure of retained δ-ferrite surrounds the prior austenite grains.

Figure 3: Sequence of phase transformations shown by an intensity plot of the ferrite/martensite (110) and Austenite (111) peaks (a) for a temperature cycle (b) characterized by heating to a peak temperature of 1573K (1300°C) with a rate of $10Ks^{-1}$ and subsequent cooling at the same rate. A plot of the evolution of the ferrite-martensite (BCC/BCT) phase fraction as a function of the thermal cycle is shown in (c).

Figure 4: Optical micrograph (a) of 9Cr steel after thermal cycling revealing martensitic matrix with skeletal and grain boundary (GB) retained δ-ferrite (bright phase) and magnified section with the origin of the skeletal morphology delineated. The arrows in (b) indicate the direction of austenite formation during cooling.

The phase fraction of retained delta ferrite was evaluated by image analysis of optical micrographs using Zeiss® KS400 Image Analysis Software. To obtain statistically relevant values, a total area of 6.3 x 4.3 mm was analyzed at a magnification of 200x. Image analysis resulted in a measured mean δ-ferrite fraction of 5.6 with a standard deviation of 1.9 %. Since the phase fractions are measured based on color differences resulting from the different etching response of δ-ferrite (bright) and martensite (dark), there is some uncertainty in the measurements. In particular, the skeletal regions of δ-ferrite are surrounded by areas of martensite with lighter etching response comparable to the δ-ferrite (see Figure 4b) and therefore might be wrongfully added to the δ-ferrite fraction. Retained austenite could not be identified in the micrographs since it is present as sub-micron sized laths (which fall below the resolution of optical microscopy) between martensite laths.

When compared to the equilibrium phase transformation temperatures, superheating on the order of 40 to 50K for the ferrite to austenite transformation is observed and attributed to the kinetic influence of the heating rate. On the contrary, the austenite to δ-ferrite transformation in the XRD experiment started about 30K below the calculated equilibrium value, which can be explained by local enrichment in chromium and molybdenum due to the dissolution of Cr-rich $M_{23}C_6$ (T_{sol}=1259K (986°C)) along the prior austenite grain boundaries. Such segregated areas rich in ferrite-stabilizing elements are preferential points for δ-ferrite nucleation.

Conclusions

XRD measurements proved to be sensitive enough in detecting even a small volume fraction of δ-ferrite and monitoring its evolution and retention. The data reveal that in the temperature range from 1305±15K (1032 ±15°C) to 1483±15K (1210 ±15°C) the steel exhibits a single-phase austenitic matrix. It is therefore possible that a fully martensitic matrix can be formed by annealing in this single-phase austenite temperature range followed by rapid cooling. A single-weld thermal cycle, characterized by an increased heating rate, low dwell time and relatively fast cooling, inhibits the achievement of this equilibrium condition. More time in the austenitic single-phase region would be needed to compensate for the inhomogeneous elemental distribution caused by the dissolution of chromium carbides.

Acknowledgements

The support of PM through the Max Kade Foundation, NY and the Austrian Academy of Sciences is gratefully acknowledged. Research sponsored by the Division of Materials Sciences and Engineering, Office of Basic Energy Sciences, U.S. Department of Energy (EDS). Use of the Advanced Photon Source at Argonne National Laboratory was supported by the U. S. Department of Energy, Office of Science, Office of Basic Energy Sciences, under Contract No. DE-AC02-06CH11357.

[1] L. Schafer: J. Nucl. Mater., 1998, Vol. 263, pp. 1336 -1339.

[2] F. Abe, T-U. Kern, R. Viswanathan (Eds.): Creep resistant steels, Woodhead Publishing Limited, Boca Raton, 2008, pp. 279-304.

[3] F. Abe, T-U. Kern, R. Viswanathan (Eds.): Creep resistant steels, Woodhead Publishing Limited, Boca Raton, 2008, pp. 472-503.

[4] H. Cerjak, HKDH Bhadeshia (Eds.): Mathematical Modelling of Weld Phenomena 5, IOM Communications, London, 2001, pp. 349-361.

[5] Thermodynamic database 'mc_steel'. Institute of Materials Science and Technology, Vienna University of Technology, Austria, 2009.

[6] J.C. Zhao, Z.P. Jin: Acta Metall. Mater., 1990, Vol. 38, pp. 425-431.

[7] J.W. Elmer, T.A. Palmer, S.S. Babu, E.D. Specht: Mat.Sci. Eng. A-Struct., 2005, Vol. 391, pp. 104-113.

[8] J.W. Elmer, T.A. Palmer, W. Zhang, B. Wood, T. DebRoy: Acta Mater., 2003, Vol 51, pp. 3333-3349.

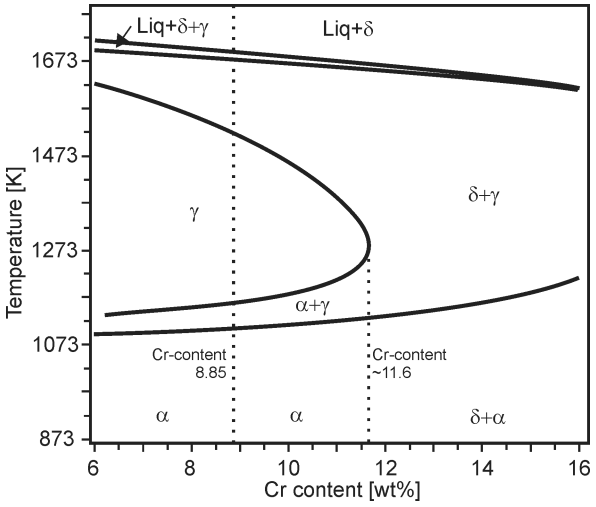

Figure 1

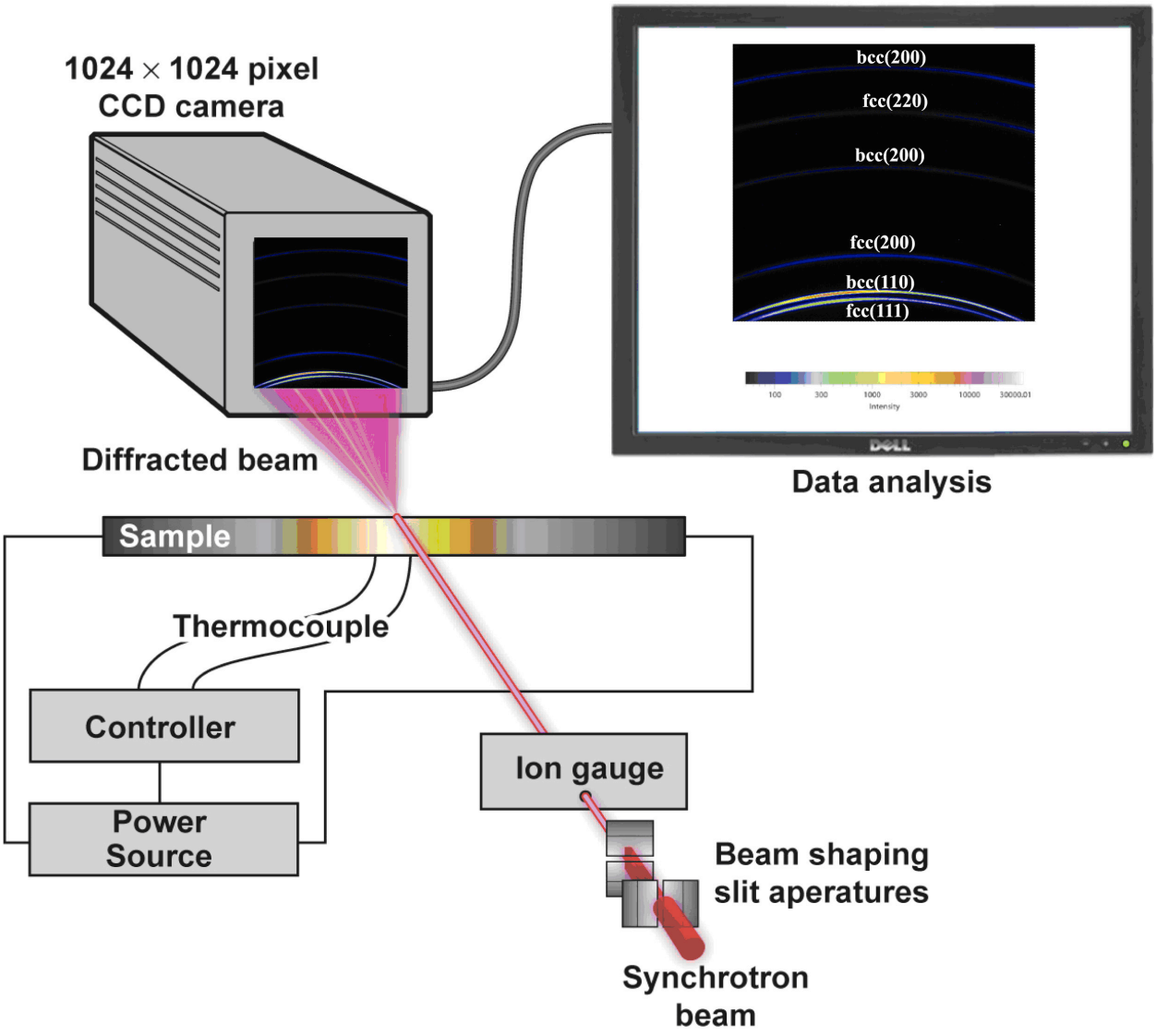
1024 × 1024 pixel
CCD camera
bcc(200)
fcc(220)
bcc(200)
fcc(200)
bcc(110)
fcc(111)
100
300
1000
3000
10000
30000.01
Intensity
DELL
Diffracted beam
Data analysis
Sample
Thermocouple
Controller
Power
Source
Ion gauge
Beam shaping
slit aperatures
Synchrotron
beam

Figure 2

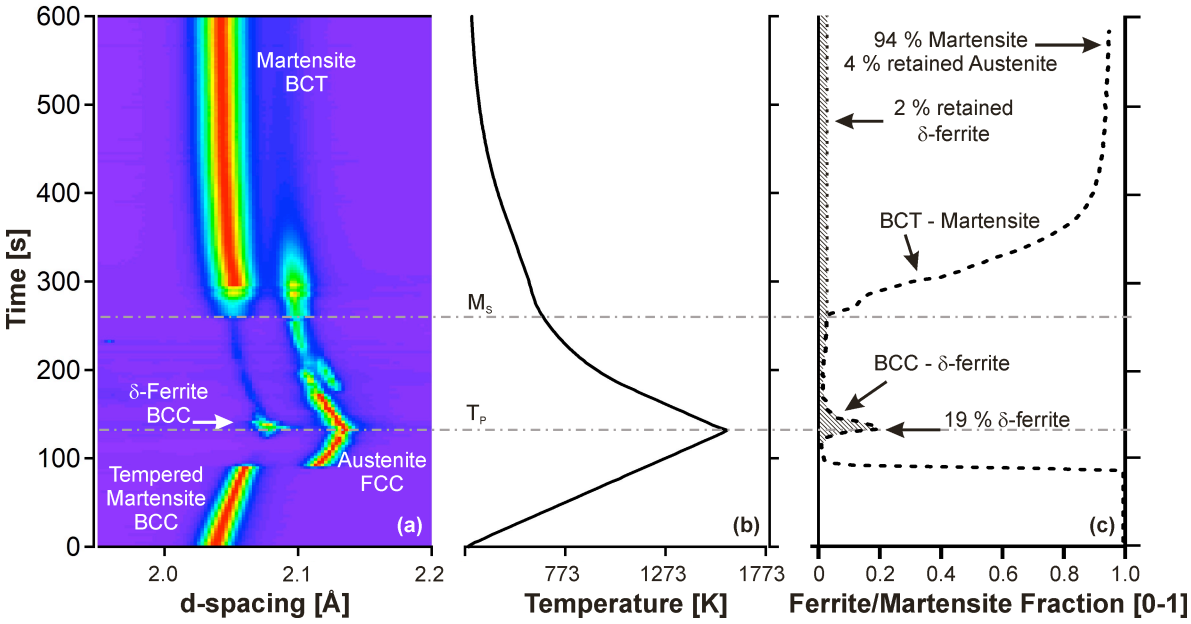

Figure 3

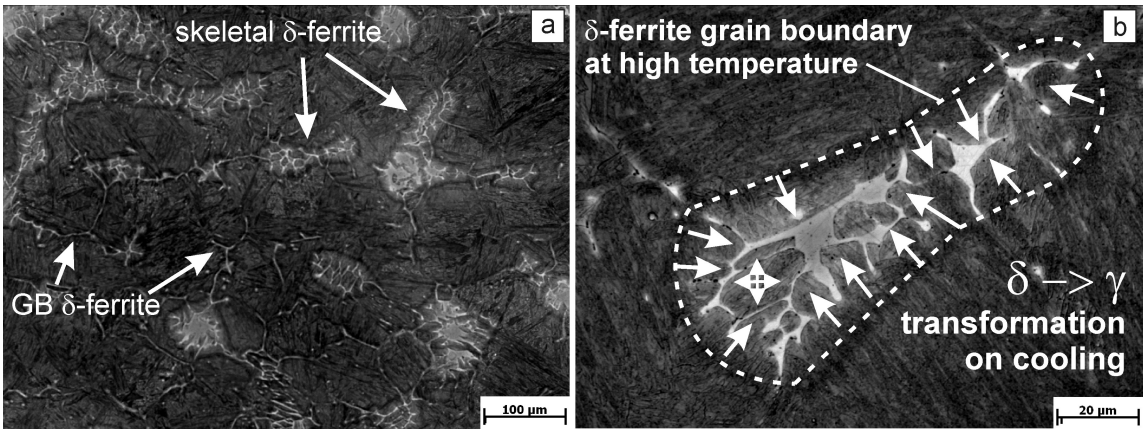

Figure 4

	A_{e1}/A_{c1}	A_{e3}/A_{c3}	A_{e4}/A_{c4}	M_S
Equilibrium	1113K (840°C)	1168K (895°C)	1512K (1239°C)	* 697K (424°C)
XRD	1153±15K (880 ±15°C)	1305±15K (1032±15°C)	1483±15K (1210 ±15°C)	676±5K (403 ±5°C)
Dilatometry	1165K (892°C)	1303K (1030°C)	1533K (1260°C)	713K (440°C)

* calculated for a driving force of 1,400 Joule/mol

Table 1